Ab Initio Calculations of Structural, Electronic, and Mechanical Stability Properties of Magnesium Sulfide

Hai-Ying Wu[a], Ya-Hong Chen[b], Ping Zhou[a], Xiang-Yu Han[a], and Zi-Jiang Liu[c]

[a] School of Science, Chongqing Jiaotong University, Chongqing 400074, China
[b] School of Chemical Engineering and Environment, North University of China, Taiyuan, 030051, China
[c] Department of Physics, Lanzhou City University, Lanzhou, 730070, China

Reprint requests to H. W.; E-mail: hywu09@163.com

Z. Naturforsch. **69a**, 403 – 410 (2014) / DOI: 10.5560/ZNA.2014-0027
Received September 12, 2013 / revised March 6, 2014 / published online June 18, 2014

The structural, electronic, and mechanical stability properties of magnesium sulfide in different phases are presented using the plane wave pseudopotential method within the generalized gradient approximation. Eight different phases such as rocksalt (B1), zincblende (B3), wurtzite (B4), nickel arsenide (B8), cesium chloride (B2), PH_4I-type (B11), FeSi-type (B28), and MnP-type (B31) are considered in great detail. The calculated ground-state properties of these phases are consistent with available experimental and theoretical data. It is found that MgS in the B1 and B8 phases are indirect band gap materials, the B3, B4, B11, B28, and B31 phases are all direct gap materials, while the B2 phase displays the metallic character. The B1, B3, B4, B8, B28, and B31 phases are mechanically stable at ambient conditions, but the B2 and B11 phases are mechanically unstable under zero pressure and zero temperature.

Key words: Magnesium Sulphide; Structural Properties; Electronic Properties; Mechanical Stability Properties.

1. Introduction

The alkaline-earth-chalcogenides (AEC) II–VI semiconductors have attracted great attention from a considerable amount of experimental and theoretical studies due to their important wide band gap character and potential applications for optoelectronic devices [1]. Among AEC materials, magnesium chalcogenides are large gap binary semiconductors (band gap values $\approx 2-3.5$ eV) that have technological applications in catalysis, opto-electronics [2], and luminescent device production [3, 4] with low dielectric constants.

Magnesium sulfide is a wide band gap semiconductor (band gap exceeds 4.5 eV at room temperature) that belongs to the magnesium chalcogenides family and is one of the least studied members. The stable crystal structure of MgS is the cubic B1 phase under ambient pressure [5]. Motivated by the technological usefulness, the remarkable and interesting physical properties, MgS has been investigated both theoretically and experimentally. The ground state properties, phase transition, electronic, elastic, and dynamical properties have been theoretically investigated [1, 6 – 17].

Despite much experimental and theoretical work, MgS is not well understood for some of its properties so far. The vast majority of researches on MgS have been focused on cubic B1, B3, and B2 crystal phases, many fundamental physical properties of this compound remain to be determined precisely. In this paper, we report a detailed calculation of the structural, electronic, and mechanical stability properties of eight different phases of MgS in order to further understand this material. We first examine the results of the calculated structural properties in the B1, B2, B3, B4, B8, B11, B28, and B31 structures at zero temperature. And then we undertake a systematic ab initio theoretical study of the electronic band structure and mechanical stability relations of these eight phases of MgS.

2. Computational Methods

The plane-wave pseudopotential approach within the framework of density functional theory (DFT) is

used in this work. All the calculations have been performed using ABINIT code [18]. The ab initio norm-conserving pseudopotentials [19] are generated using the method of Troullier and Martins [20]. The electronic exchange-correlation energy is treated within the generalized gradient approximation (GGA) of Perdew, Burke, and Ernzerhof (PBE) scheme [21] in our calculations.

The electronic wave functions are expanded in a basis set of plane waves, up to the kinetic energy cutoff of 30 hartree for the B1 structure, 50 hartree for the B3 structure and B2 structure, 40 hartree for the B4 structure, B8 structure, B28 structure, B31 structure, and B11 structure, respectively. For the k point sampling, we choose $8 \times 8 \times 8$ shifted Monkhorst–Pack mesh [22] for the B1 structure, B2 structure, and B3 structure, $12 \times 12 \times 7$ shifted Monkhorst–Pack mesh for the B4 structure and B8 structure, $6 \times 6 \times 6$ shifted Monkhorst–Pack mesh for the B28 structure, $8 \times 8 \times 6$ shifted Monkhorst–Pack mesh for the B11 structure, $6 \times 10 \times 6$ shifted Monkhorst–Pack mesh for the B31 structure, respectively. These values are tested and determined to provide convergence in self-consistent calculations. When geometry optimization is performed, the tolerance on total energy is set to 10^{-7} hartree and these parameters ensure that the tolerance on the maximal force is $5.0 \cdot 10^{-6}$ hartree/Bohr.

In order to investigate the structural parameters of all phases in details, the structure optimization process is performed by the Broyden–Fletcher–Goldfarb–

Table 1. Lattice parameters (Å), dimensionless c/a ratio, bulk modulus (GPa), and its dimensionless pressure derivative of all possible phases of MgS.

	a	b	c	c/a	B_0	B_0'
Rocksalt (B1)						
This work	5.22				74.98	3.91
Exp. [6]	5.20				82.80	3.98
Exp. [5]	5.20				76.00 ± 0.13	3.71 ± 0.34
PP-PW (LDA) [14]	5.22				74.20	3.87
PP-PW (GGA) [13]	5.23				74.20	4.18
PP-PW (GGA) [9]	5.22				76.36	3.66
PP-PW (GGA) [22]	5.23				72.64	4.78
MD-GGA [26]	5.29				89.00	3.99
Zincblende (B3)						
This work	5.68				55.16	3.92
Exp. [27]	5.64					
Exp. [7]	5.66					
PP-PW (LDA) [14]	5.67				56.22	3.22
PP-PW (GGA) [13]	5.70				55.90	4.11
PP-PW (GGA) [9]	5.68				53.84	3.63
PP-PW (LDA) [11]	5.64				60.00	4.06
Wurtzite (B4)						
This work	4.04		6.47	1.60	55.24	3.59
Exp. [28]	3.97		6.44	1.62		
PP-PW (GGA) [13]	4.07		6.42	1.58	56.10	4.27
MD-GGA [26]	4.04		6.51	1.61	63.00	3.47
Nickel arsenide (B8)						
This work	3.66		6.16	1.69	72.45	4.03
LAPW [25]	3.61		6.09	1.69	82.00	4.15
PP-PW (GGA) [13]	3.67		6.15	1.68	74.60	4.29
Cesium chloride (B2)						
This work	3.27				68.38	3.99
PP-PW (GGA) [13]	3.28				69.20	3.82
PP-PW (GGA) [22]	3.28				70.27	4.05
PH_4I-type (B11)						
This work	4.48		4.37	0.98	15.51	6.85
FeSi-type (B28)						
This work	5.22				76.20	3.85
MnP-type (B31)						
This work	6.16	3.66	6.34	1.03	75.17	3.89

Table 2. Our calculated energy band gap (eV) of MgS at equilibrium volume along with other experimental and theoretical data.

Structure	This work	Other Theoretical Calculations	Experiments
B1 ($\Gamma - X$)	2.76	2.70 (LAPW) [25], 3.61 (PP-PW) (GGA) [22], 2.21 (FP-LAPW (LDA)) [6], 2.76 (FP-LMTO) [10], 2.56 (PP-PW (LDA)) [11]	4.60 [27]
B3 ($\Gamma - \Gamma$)	3.38	3.37 (FP-LAPW (LDA)) [6], 3.10 (PP-PW (LDA)) [11], 3.42 (FP-LAPW (LSDA)) [29], 3.36 (PAW (GGA)) [12], 3.98 (PP-PW (GGA)) [22]	4.50 [28]
B4 ($\Gamma - \Gamma$)	3.39	3.15 (PP-PW (LDA)) [11], 3.50 (FP-LMTO) [10], 3.96 (PP-PW (GGA)) [22]	
B8 ($\Gamma - K$)	3.39	3.05 (PP-PW (LDA)) [11]	
B2 ($M - M$)	0.58	0.42 (PP-PW (GGA)) [22]	
B11 ($\Gamma - \Gamma$)	2.80		
B28 ($\Gamma - \Gamma$)	2.76		
B31 ($\Gamma - \Gamma$)	3.41		

Shanno (BFGS) algorithm [23]. The lattice constants and specific cell-internal dimensionless crystal parameters are all optimized during this process.

3. Results and Discussion

The structures of the eight different (B1, B3, B8, B4, B2, B11, B28, and B31) phases of MgS are plotted in Figure 1. The total energies as the function of volumes per formula in these possible structures of MgS are calculated in detail as shown in Figure 2. It is clear that MgS is stable in the B1 structure at ambient conditions. The calculated total energies are then fitted to the Birch–Murnaghan equation of state [24] to derive the equilibrium volume V_0, bulk modulus B_0, and its pressure derivative B_0'. The obtained equilibrium lattice constants, bulk modulus B_0, and its pressure derivative B_0' in all phases of MgS together with available experimental and other theoretical results are given in Table 1. Our calculated ground-state properties for the B1, B3, B4, B8, and B2 phases are found to be in good agreement with available experimental and theoretical data. Unfortunately, there are no available experimental and theoretical data in the B11, B28, and B31 structures of MgS for comparison so far.

The calculated equation of state (EOS) of MgS in all phases is displayed in Figure 3. The insets in this figure display our calculated EOS in the B1 structure and that of Peiris et al. [5] by means of a diamond anvil cell up to a pressure of 54 GPa. It is to be noted that our results agree well with the experimental data of Peiris et al. Furthermore, the B11 structure is the most easy while the B8 structure is the most difficult to be compressed phase when the pressure increases.

As the compound with a large diversity of physical properties related to the energy band structure, the electronic structures of MgS have been investigated by different experimental and theoretical methods [6, 28 – 31]. Analysis of the electronic band structure of MgS suggests an indirect band gap in the B1 structure and a direct band gap in the B3 structure. Little work has been done to investigate the electronic structure of MgS in other phases. Based on the crystal parameters obtained above, the calculated electronic band structures and density of states (DOS) of MgS in different phases (B1, B3, B8, B4, B2, B11, B28, and B31) at ambient conditions are presented in detail. Our calculated results also demonstrate that MgS exhibits indirect band gap in the B1 structure with band gap occurring between Γ and X points which is also found for other II–VI compounds [32, 33] and direct band gap in the B3 structure with band gap occurring between Γ and Γ points as shown in Figures 4 and 5. These results are consistent with the former experimental and theoretical conclusion. Moreover, it is found that the B4, B11, B28, and B31 phases are all direct band gap materials with band gap occurring between Γ and Γ points as shown in Figures 6 – 9, respectively. The B2 phase is metallic because of the finite DOS at the Fermi level. Moreover, due to the small values of DOS at the Fermi energy level, the B2 phase is a poor conductor as shown in Figure 10. This result is in contrast with the semiconductor character of the B2 phase for other II–VI semiconductors such as SrS, SrSe, and SrTe [32]. In addition, the B8 phase of MgS is an indirect band gap material with band gap occurring between Γ and K points as shown in Figure 11. Our calculated band gap values and the estimates of band gap width of MgS given in the literatures are summarized in Table 2. It is

noted that our calculated band gap values are in excellent accordance with similar theoretical results. Our calculated band gap values are slightly less than the experimental works. The difference may be due to the neglect of the excited state calculation and GGA usually underestimate the energy gap because GGA have simple forms that are not sufficiently flexible for accurately reproducing both exchange-correlation energy and its charge derivative [33, 34].

Recently, the elastic constants and mechanical stabilities of crystals have attracted much interest. The knowledge of elastic constants of a crystal provides access to understand the mechanical properties for practical application in many fields, e. g. fracture toughness, sound velocity, anisotropy, etc. Therefore, in order to further verify the mechanical stability of the eight polymorphs of MgS, the complete set of zero pressure elastic constants for these eight structures are calculated. The calculated elastic constants along with previous experimental and theoretical data are listed in Table 3. Our calculated elastic constants of MgS in the B1 and B3 structure at zero pressure are consistent with the experimental data and other calculated results. Unfortunately, there are no available experimental and theoretical elastic constants for the other six structures of MgS been obtained up to now.

For a cubic crystal, the mechanical stability requires the following conditions to be satisfied: $(C_{11} - -C_{12}) > 0$, $(C_{11} + 2C_{12}) > 0$, $C_{11} > 0$, $C_{44} > 0$ [35]. As shown in Table 3, the presented elastic constant values of cubic B1, B3, and B28 structure satisfy the conditions of mechanical stability mentioned above, assuring the mechanical stability of the B1, B3, and B28 structure of MgS. While at ambient condition the calculated elastic constants of the B2 structure do not meet the criteria of mechanical stability of cubic crystal, and this means that the B2 structure of MgS is mechanically unstable at ambient condition. However, the B2 structure of other II–VI semiconductors such as barium chalcogenides and strontium chalcogenides is mechanically stable at ambient condition [32, 33].

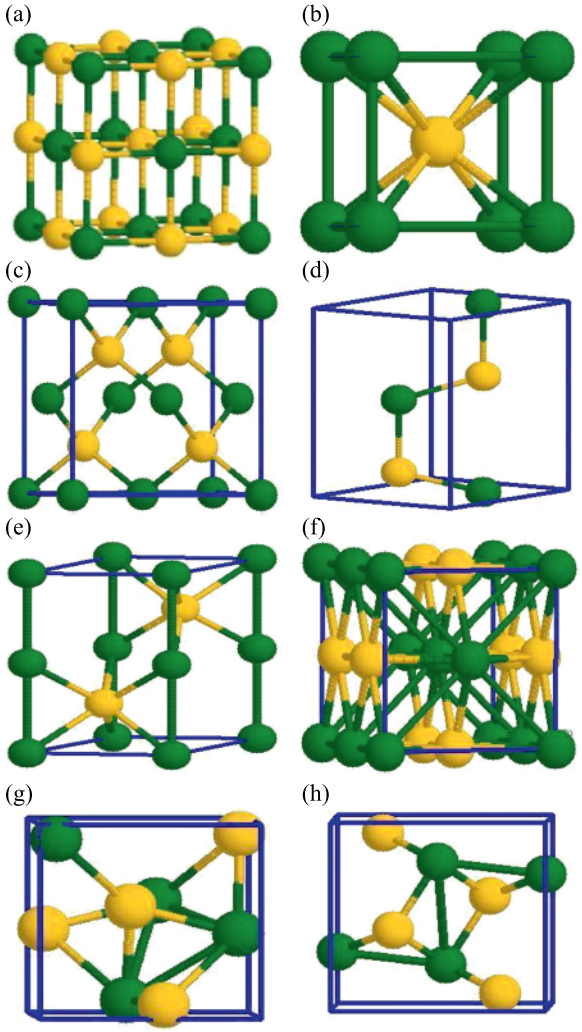

Fig. 1 (colour online). Structures of the eight different phases (a) B1, (b) B2, (c) B3, (d) B4, (e) B8, (f) B11, (g) B28, (h) B31 of MgS.

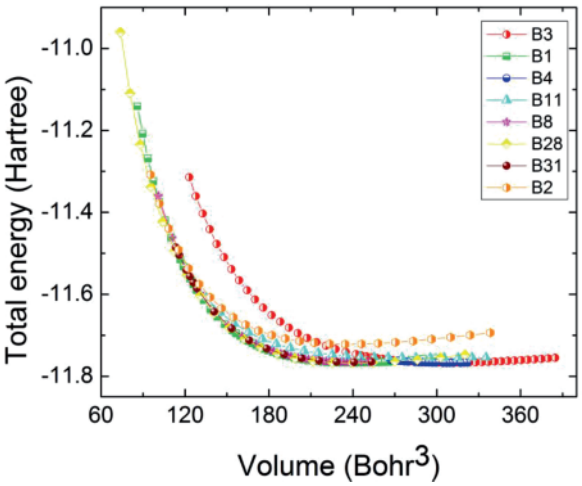

Fig. 2 (colour online). Calculated total energies as a function of volumes per formula of MgS.

Table 3. Calculated elastic constants (GPa) of all possible structures of MgS at ambient conditions.

	C_{11}	C_{12}	C_{13}	C_{22}	C_{23}	C_{33}	C_{44}	C_{55}	C_{66}
Rocksalt (B1)									
This work	137.80	41.04					54.67		
PP-PW (LDA) [14]	168.40	42.20					55.20		
PP-PW (GGA) [13]	134.50	44.10					56.70		
FP-LAPW (LDA) [6]	183.45	34.90					69.01		
Zincblende (B3)									
This work	69.53	47.45					30.37		
PP-PW (LDA) [14]	74.00	54.80					28.24		
PP-PW (GGA) [13]	74.20	51.23					34.76		
FP-LAPW (LDA) [6]	72.37	55.76					58.41		
Wurtzite (B4)									
This work	84.24	45.16	38.66			80.71	19.11		19.54
Nickel arsenide (B8)									
This work	136.05	50.83	26.15			175.67	33.18		42.61
Cesium chloride (B2)									
This work	43.06	−17.33					−23.04		
PH_4I-type (B11)									
This work	41.37	70.55	7.23			9.97	10.64		57.35
FeSi-type (B28)									
This work	137.91	41.02					54.65		
MnP-type (B31)									
This work	175.84	26.20	26.16	136.30	50.91	136.16	42.66	33.19	33.24

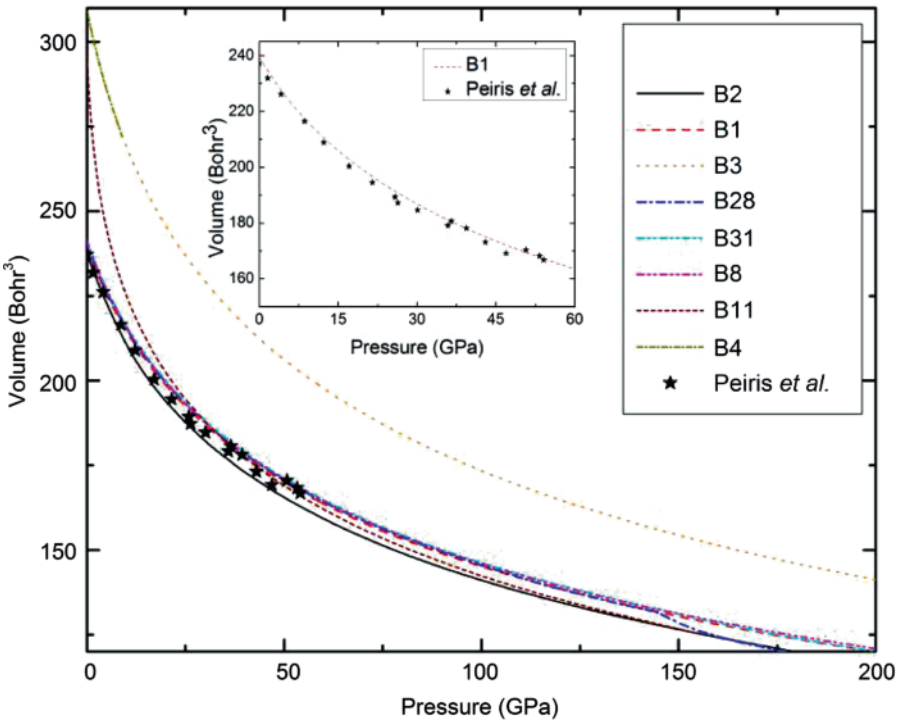

Fig. 3 (colour online). Calculated equation of state (EOS) in all structures of MgS.

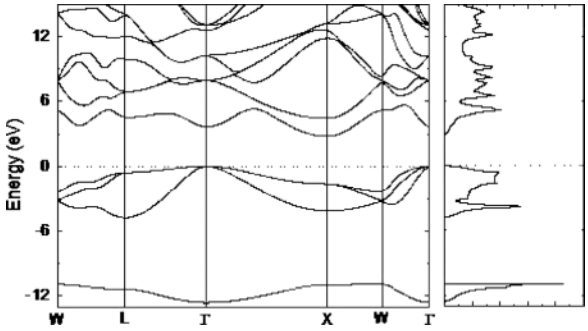

Fig. 4. Calculated electronic band structure and density of state of MgS in the B1 structure.

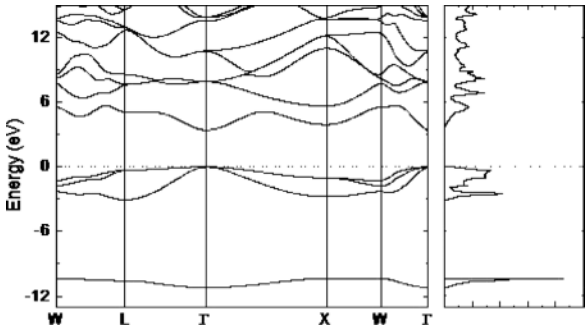

Fig. 5. Calculated electronic band structure and density of state of MgS in the B3 structure.

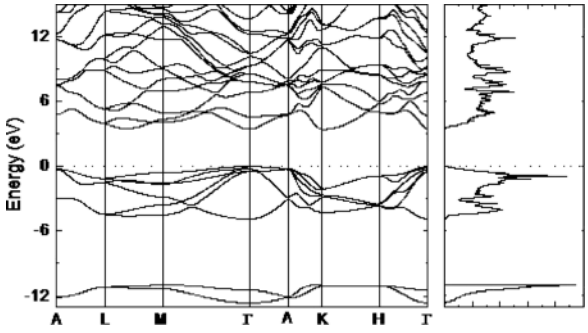

Fig. 6. Calculated electronic band structure and density of state of MgS in the B4 structure.

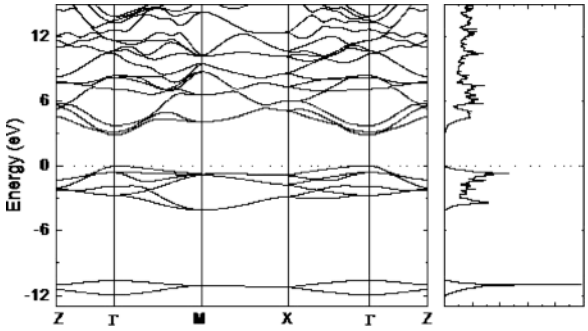

Fig. 7. Calculated electronic band structure and density of state of MgS in the B11 structure.

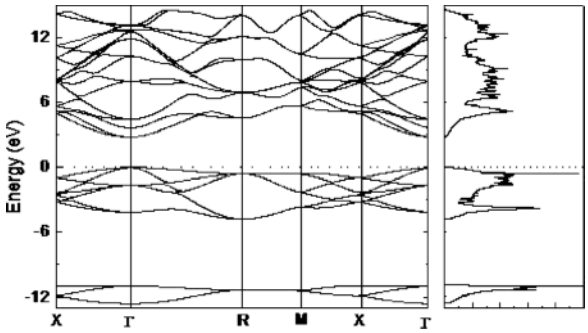

Fig. 8. Calculated electronic band structure and density of state of MgS in the B28 structure.

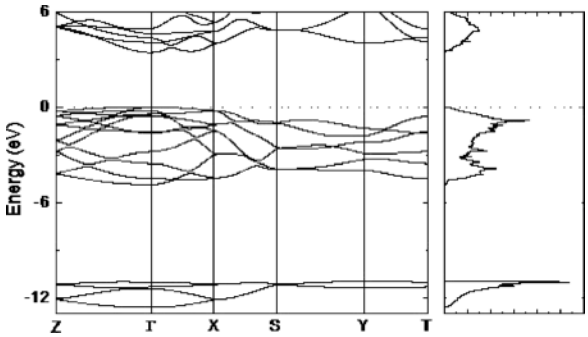

Fig. 9. Calculated electronic band structure and density of state of MgS in the B31 structure.

For a hexagonal crystal, the criteria for mechanical stability are given by $C_{44} > 0$, $C_{11} > |C_{12}|$, $C_{33}(C_{11} + C_{12}) > 2C_{13}^2$ [35]. It can be noted that our calculated elastic constants of MgS for the B4 and B8 structure all satisfy the conditions for mechanical stability of a hexagonal crystal, implying the mechanical stability of the B4 and B8 structure of MgS at zero pressure.

For a tetragonal crystal, the mechanical stability is judged by the following condition: $C_{11} > 0$, $C_{33} > 0$, $C_{44} > 0, C_{66} > 0, (C_{11} - C_{12}) > 0, (C_{11} + C_{33} - 2C_{13}) > 0$, $[2(C_{11} + C_{12}) + C_{33} + 4C_{13})] > 0$ [35]. The values of elastic constants for the B11 structure of MgS at zero pressure from Table 3 do not fulfill the mechanical stability criteria mentioned above. This indicates that the B11 structure of MgS is not a mechanically stable structure at zero pressure.

For an orthorhombic crystal, the elastic constants should satisfy the following inequalities: $C_{11} > 0$,

$C_{22} > 0$, $C_{33} > 0$, $C_{44} > 0$, $C_{55} > 0$, $C_{66} > 0$, $[C_{11} + C_{22} + C_{33} + 2(C_{12} + C_{13} + C_{23})] > 0$, $(C_{11} + C_{22} - 2C_{12}) > 0$, $(C_{11} + C_{33} - 2C_{13}) > 0$, $(C_{22} + C_{33} - 2C_{23}) > 0$ [35]. According to the above criteria, it is clear that MgS within the B31 structure is also mechanically stable under normal conditions.

4. Conclusions

The structural, electronic, and mechanical stability properties of MgS within eight considered structures have been studied using first principles calculations. Our calculated ground-state properties for these eight phases are in good agreement with available experimental and theoretical results. The obatined band structure and DOS results demonstrate that MgS is the indirect band gap in the B1 phase and B8 phase. Moreover, it is found that the B3, B4, B11, B28, and B31 phases are all direct gap materials, while the B2 phase is metallic and a poor conductor. Our calculated band gap values for these phases of MgS are consistent with available experimental and other theoretical estimates of the band gap width given in the literatures. We find that the cubic B1, B3, and B28 phase of MgS is mechanically stable, while the cubic B2 phase is mechanically unstable at ambient conditions. The hexagonal B4 and B8 phase and the orthorhombic B31 phase of MgS are all mechanically stable at zero pressure and zero temperature. But the tetragonal B11 phase of MgS is not a mechanically stable structure at zero pressure.

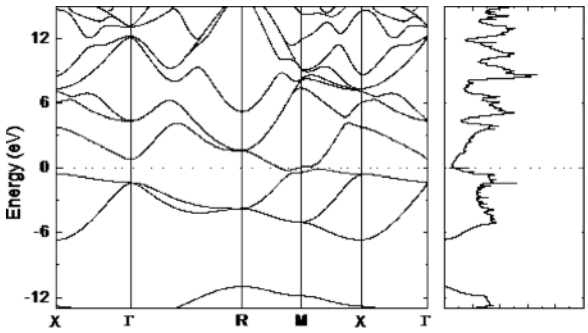

Fig. 10. Calculated electronic band structure and density of state of MgS in the B2 structure.

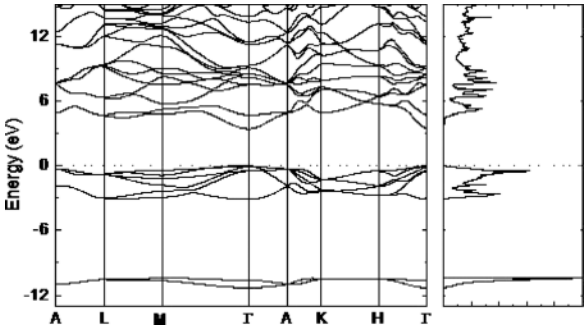

Fig. 11. Calculated electronic band structure and density of state of MgS in the B8 structure.

Acknowledgements

This research is financially supported by the National Natural Science Foundation of China under grant No. 11064007 and the New Century Excellent Talents in University under grant No. NCET-11-0906. The authors thank Dr. X. Gonze and his coworkers for providing us their version of ABINIT code.

[1] D. Varshney, N. Kaurav, U. Sharma, and R. K. Singh, J. Phys. Chem. Solids **69**, 60 (2008).
[2] M. W. Wang, M. C. Phillips, J. F. Swenberg, E. T. Yu, J. O. McCaldin, and T. C. McGill, J. Appl. Phys. **73**, 4660 (1993).
[3] H. G. Zimmer, H. Winze, and K. Syassen, Phys. Rev. B **32**, 4066 (1985).
[4] R. Pandey and S. Sivaraman, J. Phys. Chem. Solids **52**, 211 (1991).
[5] S. M. Peiris, A. J. Campbell, and D. L. Heinz, J. Phy. Chem. Solids **55**, 413 (1994).
[6] F. Drief, A. Tadjer, D. Mesri, and H. Aourag, Catal. Today **89**, 343 (2004).
[7] L. Konczewicz, P. Bigenwald, T. Cloitre, M. Chibane, R. Ricou, P. Testud, O. Briot, and R. L. Aulombard, J. Cryst. Growth **159**, 117 (1996).
[8] A. Chakrabarti, Phys. Rev. B **62**, 1806 (2000).
[9] F. A. Sahraoui, S. Zerroug, L. Louail, and D. Maouche, Mater. Lett. **61**, 1978 (2007).
[10] D. Rached, N. Benkhettou, B. Soudini, B. Abbar, N. Sekkal, and M. Driz, Phys. Status Solidi B **240**, 565 (2003).
[11] S. Duman, S. Bağcl, H. M. Tütüncü, and G. P. Srivastava, Phys. Rev. B **73**, 205201 (2006).
[12] G. Gökoğlu, M. Durandurdu, and O. Gülseren, Comput. Mater. Sci. **47**, 593 (2009).
[13] H. Z. Fu, W. F. Liu, and T. Gao, Phys. Status Solidi B **247**, 48 (2010).
[14] S. Saib, N. Bouarissa, P. Rodríguez-Hernández, and A. Muñoz, Eur. Phys. J. B **73**, 185 (2010).
[15] P. Jha, U. K. Sakalle, and S. P. Sanyal, J. Phys. Chem Solids **59**, 599 (1998).

[16] Y. D. Guo, Z. J. Yang, Q. H. Gao, and W. Dai, Physica B **403**, 2367 (2008).
[17] Z. J. Chen, Acta Phys. Sin. **61**, 177104 (2012).
[18] X. Gonze, J.-M. Beuken, R. Caracas, F. Detraux, M. Fuchs, G.-M. Rignanese, L. Sindic, M. Verstraete, G. Zerah, F. Joller, M. Torrent, A. Roy, M. Mikami, Ph. Ghosez, J.-Y. Raty, and D. C. Allan, Comput. Mater. Sci. **25**, 478 (2002).
[19] W. C. Topp and J. J. Hopfield, Phys. Rev. B **7**, 1295 (1973).
[20] N. Troullier and J. L. Martins, Phys. Rev. B **43**, 1993 (1991).
[21] J. P. Perdew, K. Burke, and M. Ernzerhof, Phys. Rev. Lett. **77**, 3865 (1996).
[22] H. J. Monkhorst and J. D. Pack, Phys. Rev. B **13**, 5188 (1976).
[23] W. H. Press, B. P. Flannery, S. A. Teukolsky, and W. T. Vetterling, Numerical Recipes: The Art of Scientific Computing (FORTRAN Version), Cambridge Univ. Press, New York 1989.
[24] F. Birch, Phys. Rev. **71**, 809 (1947).
[25] Z. J. Chen, H. Y. Xiao, and X. T. Zu, Acta. Phys. Sin. **54**, 5301 (2005).
[26] M. Durandurdu, J. Phys. Condens. Matter **21**, 452204 (2009).
[27] C. Bocchi, A. Catellani, F. Germini, L. Nasi, J. K. Morrod, K. A. Prior, and G. Calestani, Phys. Rev. B **79**, 235310 (2009).
[28] V. S. Stepanyuk, A. A. Grigorenko, A. A. Katsnelson, O. V. Farberovich, A. Szasz, and V. V. Mikhailin, Phys. Status Solidi B **174**, 289 (1992).
[29] M. Rabah, B. Abbar, U. Al-Douri, B. Bouhafs, and B. Sahraoui, Mater. Sci. Eng. B **100**, 163 (2003).
[30] A. N. Kravtsova, I. E. Stekhin, A. V. Soldatov, X. Liu, and M. E. Fleet, Phys. Rev. B **69**, 134109 (2004).
[31] H. Okuyama, K. Nakano, T. Miyajima, and K. Akimoto, Jpn. J. Appl. Phys. **30**, 1620 (1991).
[32] R. Khenata, H. Baltache, M. Rérat, M. Driz, M. Sahnoun, B. Bouhafs, and B. Abbar, Physica B **339**, 208 (2003).
[33] A. Bouhemadou, R. Khenata, F. Zegrar, M. Sahnoun, H. Baltache, and A. H. Reshak, Comput. Mater. Sci. **38**, 263 (2006).
[34] P. Dufek, P. Blaha, and K. Schwarz, Phys. Rev. B **50**, 7279 (1994).
[35] Z. J. Wu, E. J. Zhao, H. P. Xiang, X. F. Hao, X. J. Liu, and J. Meng, Phys. Rev. B **76**, 54115 (2007).